NANO LETTERS

pubs.acs.org/NanoLett Letter

Pulsed Interleaved MINFLUX

Luciano A. Masullo,[▽] Florian Steiner,[▽] Jonas Zähringer, Lucía F. Lopez, Johann Bohlen, Lars Richter, Fiona Cole, Philip Tinnefeld,* and Fernando D. Stefani*

Cite This: https://dx.doi.org/10.1021/acs.nanolett.0c04600 Read Online

ACCESS | Metrics & More | Article Recommendations | Supporting Information

ABSTRACT: We introduce p-MINFLUX, a new implementation of the highly photon-efficient single-molecule localization method with a simplified experimental setup and additional fluorescence lifetime information. In contrast to the original MINFLUX implementation, p-MINFLUX uses interleaved laser pulses to deliver the doughnut-shaped excitation foci at a maximum repetition rate. Using both static and dynamic DNA origami model systems, we demonstrate the performance of p-MINFLUX for single-molecule localization nanoscopy and tracking, respectively. p-MINFLUX delivers 1−2 nm localization precision with 2000−1000 photon counts. In addition, p-MINFLUX gives access to the fluorescence lifetime enabling multiplexing and super-resolved lifetime imaging. p-MINFLUX should help to unlock the full potential of innovative single-molecule localization schemes.

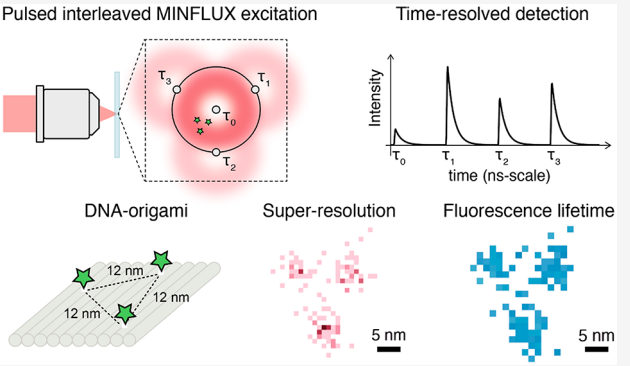

KEYWORDS: *fluorescence, super-resolution microscopy, DNA origami, single-molecule spectroscopy*

INTRODUCTION

Super-resolution fluorescence microscopy, also known as far-field fluorescence nanoscopy, has revolutionized biological imaging, because it keeps the advantages of fluorescence microscopy while delivering subdiffraction, theoretically unlimited, spatial resolution.[1−3] The first generation of super-resolution methods, which includes scanning methods, such as STED,[4,5] and wide-field single-molecule localization microscopy (SMLM) methods such as STORM[6] and PALM,[7,8] typically reaches lateral resolutions in the range of 20−50 nm, limited by fluorophore photostability. Axial resolution is normally 2-fold to 3-fold worse, in the range of 60−120 nm. More recently, this limitation was partly overcome by DNA-PAINT,[9,10] reaching lateral resolutions of <10 nm.[11,12] Imaging with this level of resolution is already enabling the characterization of subcellular structures and pathways in their natural environment with nanometric resolution, and the discovery of supramolecular protein structures.[13] Still, an extra push to the resolution limit was necessary to reach the ultimate resolution of a fluorescence microscope, namely, the molecular size of the fluorescent marker. This was achieved using a technique called MINFLUX (MINimal emission FLUXes),[14] which is a new strategy that combines structured illumination and single-molecule localization to extract maximum positional information of a single molecule using minimal photon counts. MINFLUX can routinely deliver a localization precision of ∼1 nm both in imaging and tracking of single molecules. It has been demonstrated in model systems (DNA origami structures),[14−16] fixed and living cells,[14,16,17] and it was recently extended to three dimensions.[16] While MINFLUX has represented a breakthrough, its widespread use has been slowed, because of the high technical complexity of its experimental implementation.

Here, we present pulsed interleaved MINFLUX (p-MINFLUX), which is a novel experimental realization of MINFLUX that is easier to implement in existing confocal microscopes equipped with a time-correlated single-photon counting (TCSPC) detection, only by modifying the excitation path of the microscope. No fast-scanning optics or field-programmable gate array (FPGA) electronics are required. Moreover, compared to the original MINFLUX, p-MINFLUX has the additional advantage of giving access to excited-state lifetime information, which is a relevant parameter in single-molecule spectroscopy, because it enables multiplexing of single-color measurements[18] and provides information about the environment of the fluorophore and its interactions with other molecules or materials.[19,20]

Received: November 19, 2020
Revised: December 14, 2020

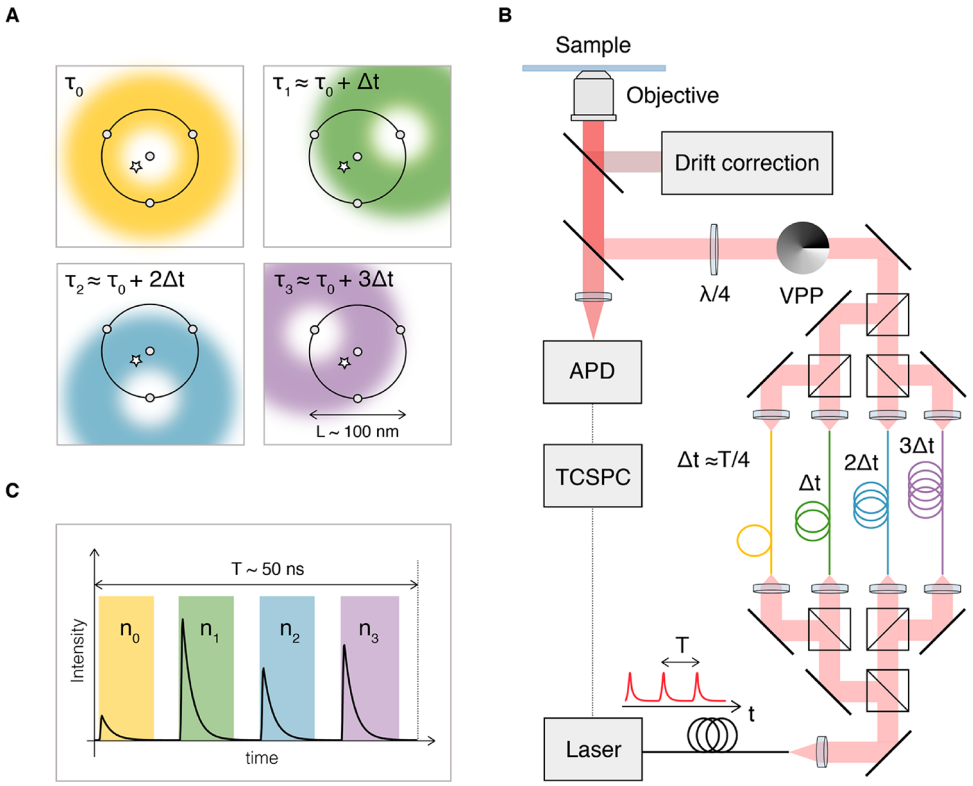

Figure 1. Description of the p-MINFLUX concept and the experimental system. (A) Four pulsed interleaved doughnut-shaped beams are focused on the sample arranged in a triangular pattern, with the fourth beam placed at the center of the triangle. The arrival time of each pulse is denoted as τ_i. The position of a single fluorescent molecule located between the laser spot positions is indicated by a star. (B) Schematic of the p-MINFLUX setup detailing the excitation pathway used to generate the pulsed interleaved doughnut foci delayed by Δt. (C) Schematic signal of detected photon counts within one period (T) of the original laser source.

WORKING PRINCIPLE AND EXPERIMENTAL SETUP

MINFLUX interrogates the position of single fluorescent molecules with a sequence of spatially displaced minima (ideally zeroes) of intensity. Figure 1A schematically shows the sequence and spatial distribution of the four doughnut-shaped foci used in this work for two-dimensional (2D) localization of single molecules. The four doughnut foci define an effective field of view of almost circular shape with a diameter L below the diffraction limit. Previous implementations of MINFLUX used the same excitation scheme, produced by shifting a continuous-wave beam between the four positions with an electro-optic scanner. By contrast, in p-MINFLUX, the excitation pattern is generated with interleaved laser pulses.[21] Figure 1B shows a schematic of the experimental setup, whose core is a confocal fluorescence microscope with modifications in the excitation path. The excitation beam is divided into four using beam splitters. Each beam is coupled into an optical fiber of different length, set to introduce time delays (Δt) of $T/4$ between the beams. The resulting arrival times of the four pulses are $\tau_i = \tau_0 + i\Delta t$, making the interleaved pulses evenly delayed within one period of the original pulse train T. For our laser source with a repetition rate of $f = 20$ MHz ($T = 50$ ns), the time delay between each one of the four excitation pulses is set to 12.5 ns ($T/4$). After outcoupling from the fibers, the four time-delayed beams are collimated. Each beam path has independent mirrors that allow the spatial alignment of the four doughnut-shaped foci into the MINFLUX excitation pattern. The four beams are recombined and passed through a $0-2\pi$ vortex phase plate (VPP) and polarization optics to create doughnut-shaped foci at the sample with a microscope objective. Further details of the setup and the control software are provided in Supplementary Section 1 in the Supporting Information.

The relative position between sample and objective is stabilized with an XYZ active drift correction by imaging fiducial nanoparticles with an independent camera. The position of the fiducial nanoparticles is recorded and eventually used for post-processing drift corrections (see Supplementary Section 2 and Figure S2A in the Supporting Information).

The detection path of the setup presents no differences from a time-resolved confocal microscope. Fluorescence from the sample is spectrally selected using conventional dichroic beam splitters and band-pass filters, and detected with an avalanche photodiode (APD). The photon counts from the APD are read out with a time-correlated single-photon counting (TCSPC) device synchronized with the laser source. In this way, detection time windows within the period T can be defined for each one of the excitation pulses (Figure 1C). Integrating the photon counts of the detection windows, an array of counts $\overline{n} = (n_0, n_1, n_2, n_3)$ is obtained, which, in turn, delivers the position of the emitter through a maximum likelihood estimation. Naturally, the excited-state lifetime information is also readily available as the photon arrival times from the four detection time windows can be combined. The setup is controlled with a dedicated open-source software written in Python, called PyFLUX (details in Supplementary Section 1 in the Supporting Information). A custom-written software was used to analyze the TCSPC data to obtain the MINFLUX position estimations of the emitter.

https://dx.doi.org/10.1021/acs.nanolett.0c04600
Nano Lett. XXXX, XXX, XXX−XXX

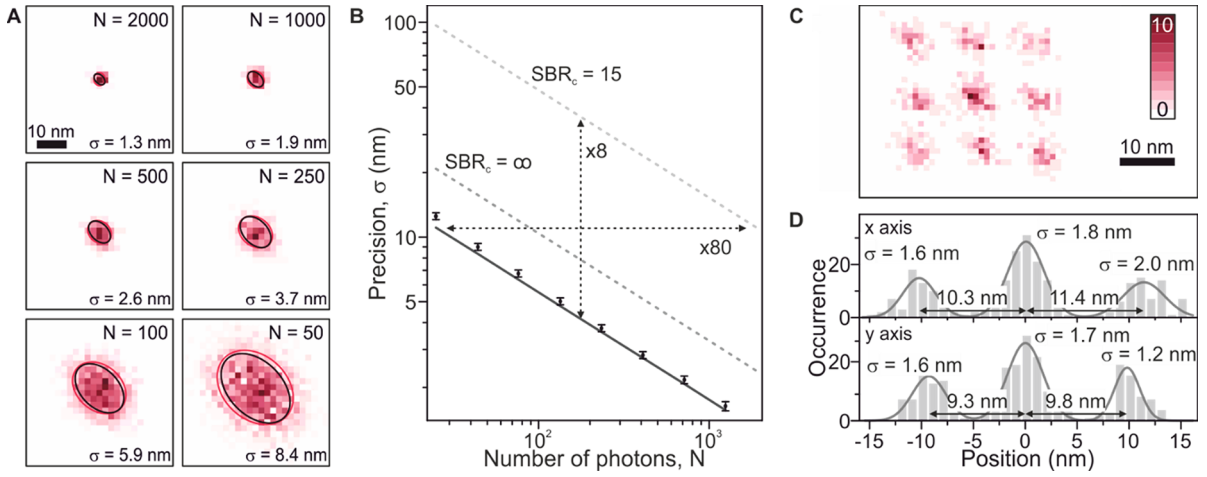

Figure 2. Evaluation of the localization performance of p-MINFLUX. (A) 2D localization histograms of a fixed single ATTO 532 dye for different number of photons, N, used to estimate the position. The red and black ellipses display the covariance of the experimental data and the Cramér-Rao bound, respectively. In this measurement, the SBR was ~15 and $L \approx 120$ nm. (B) Localization precision as a function of collected photons, N, and the Cramer-Rao-Bound (CRB) as a lower limit for the uncertainty of p-MINFLUX (black). The CRB for a camera-based localization technique for SBR = 15 and SBR = ∞ are shown in gray. (C) Localization histogram of a single GattaBead displaced by 10 nm steps in a 3 × 3 grid by using a piezo-positioner. Average $N = 2000$. (D) Cross-section along the central x-axis (top) and central y-axis (bottom) from the localization image shown in panel (C).

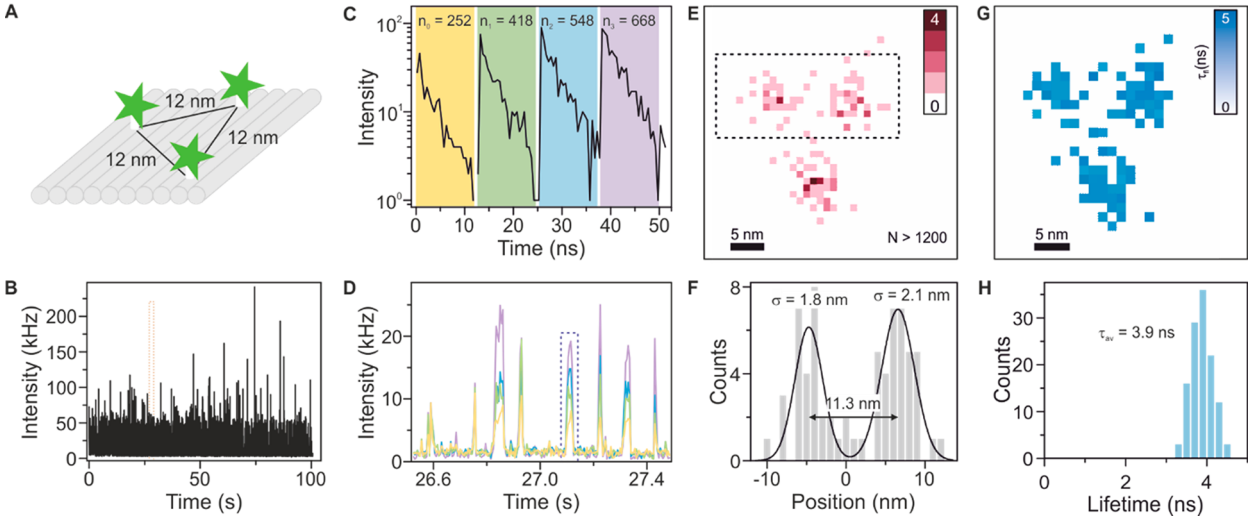

Figure 3. Super-resolution imaging with p-MINFLUX. (A) Schematic of the DNA origami structure with three ATTO 532 dyes in a triangular array. (B) 100 s trace of the total fluorescence intensity of a single DNA origami structure. In this measurement, the SBR was ~8. (C) Fluorescence decays and total integrated counts on the four detection channels for the single-molecule emission event marked in panel (D). (D) Expanded view of the time trace shown in panel (B). The intensity is split into the four detection time windows, corresponding to the four excitation beams (color-coded as in Figure 3C). (E) 2D localization image for one DNA origami structure. Single-molecule emission events with $N < 1200$ were discarded. (F) Average horizontal profile of localizations from the area marked in E. (G) p-MINFLUX fluorescence lifetime image. (H) Distribution of fluorescence lifetimes for all localizations in panel (E).

LOCALIZATION PRECISION, NANOSCOPY, AND TRACKING

The localization precision of p-MINFLUX as a function of the number of detected photons (N) was tested using single ATTO 532 molecules fixed to a DNA origami nanostructure (further details about DNA origami folding and the measurement protocol are described in Supplementary Sections 3−6, Supplementary Tables 1 and 2, in the Supporting Information). Figure 2A shows 2D histograms of position estimations using N ranging from 50 to 2000. As expected, MINFLUX is extremely photon efficient for localizing molecules. For example, the experimental standard deviation of localizations using $N = 50$ is $\sigma = 8.4$ nm, comparable to state-of-the-art PALM/STORM experiments, where $N = 5000$ photons are needed to achieve a precision of 8−10 nm (further details are given in Supplementary Section 7 in the Supporting Information).[22−24] With moderately high counts of $N = 1000$, the localization precision reaches $\sigma \approx 1$ nm. The experimental precision (covariance) is plotted as red ellipses and shows that the performance of p-MINFLUX closely follows the theoretically predicted Cramér-Rao bound (CRB, black ellipses) (details in Supplementary Section 7 in the Supporting Information). Figure 2B shows σ as a function of N. For comparison, curves of the experimental localization precision σ vs N for camera-based SMLM under infinite signal-to-background ratio (SBR = ∞) and under a realistic

https://dx.doi.org/10.1021/acs.nanolett.0c04600
Nano Lett. XXXX, XXX, XXX−XXX

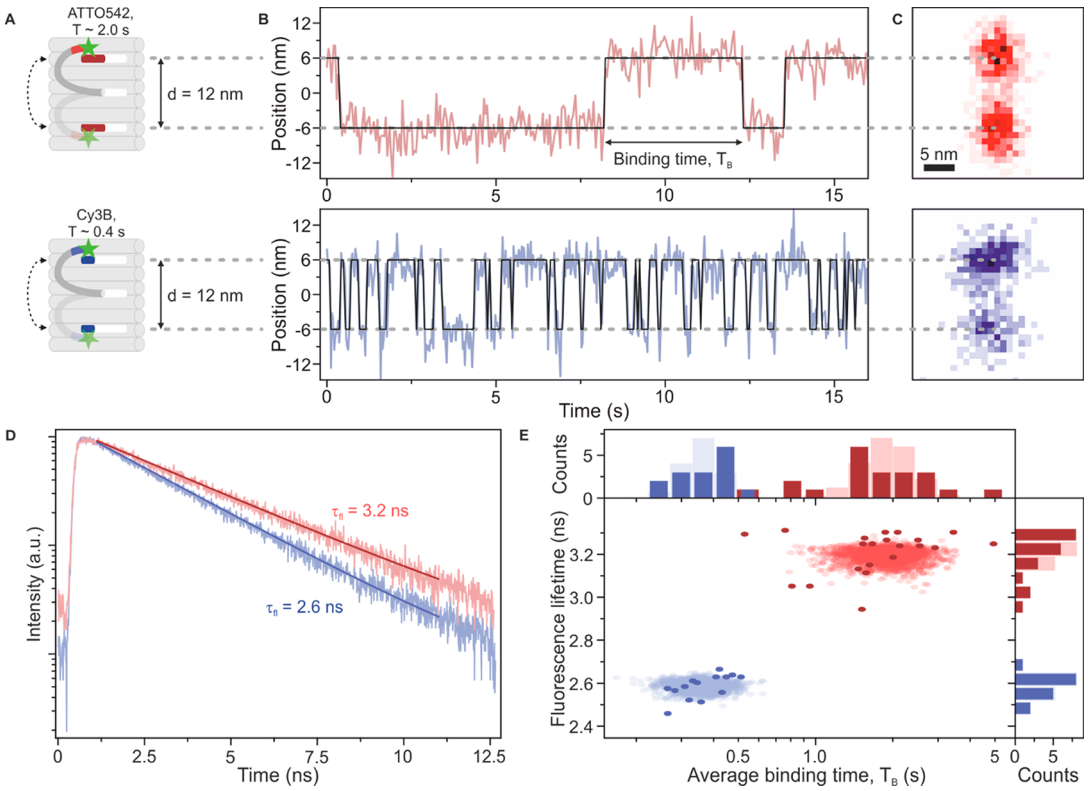

Figure 4. Molecular scale tracking of a DNA pointer on top of a DNA origami structure. (A) Schematics, (B) localization trace (binning time = 100 ms for the upper and 60 ms for the lower trace; SBR ≈ 8 for the upper trace and SBR ≈ 10 for the lower trace), and (C) 2D localization histograms of a DNA origami pointer labeled with a single ATTO 542 (upper row) and Cy3B (lower row) dye. (D) Exemplary single-molecule fluorescence decays for ATTO 542 (red) and Cy3B (blue) labeled structures. (E) Scatter plot of the average binding time T_B and fluorescence lifetime τ_{fl} obtained from the measurements on the DNA origami structures (dark red, dark blue) and from simulations (light red, light blue). The corresponding histograms for T_B and τ_{fl} are shown on top and on the right, respectively.

assumption of SBR = 15 are also depicted in Figure 2B. For the same number of detected photons, p-MINFLUX delivers almost 1 order of magnitude better localization precision than camera-based SMLM techniques. Conversely, almost 2 orders of magnitude fewer photons are needed in order to achieve the same precision as with camera-based SMLM techniques. In terms of localization precision, p-MINFLUX demonstrates an equivalent performance to the original MINFLUX microscope, given equivalent experimental conditions (L, N, SBR). This is expected because both methods work under the same principle of localization of single emitters.

The localization accuracy of p-MINFLUX was evaluated by localizing a single GattaBead (nanoparticle diameter of 23 nm, containing ATTO 542, fluorescence lifetime = 3.2 ns) as it was displaced using a piezo-positioner over a square grid with a step size of d = 10 nm. The 2D localization histogram at an average number of N = 2000 photons for each localization is shown in Figure 2C. Figure 2D shows the average profiles of the central row and the central column. The distance between the positions is $d \approx 10$ nm, which is in good agreement both with the set step size of the piezo-positioner and with the positions of the fiducial markers determined independently to correct for sample drift during the measurements (for details, see Figure S2B in the Supporting Information).

The working principle of p-MINFLUX was also evaluated through numerical simulations described in Supplementary Section 8 in the Supporting Information. The simulation results shown in Supplementary Section 9 in the Supporting Information show that the performance of p-MINFLUX is only weakly influenced by misalignments of the excitation beam pattern. For example, a lateral misalignment of any, or all four doughnut foci of up to15 nm deteriorates the localization precision by less than 1 nm (Figure S5 in the Supporting Information). We have also evaluated the effect on localization precision and accuracy of possible cross-talk between the detection time windows for different lifetimes (Supplementary Section 10 in the Supporting Information). Generally, this cross-talk may deteriorate the localization precision and/or introduce a localization bias. However, these effects are <1 nm for lifetimes smaller than 25% of the detection time windows (3 ns in our case), and are <2 nm for lifetimes up to 33% of the detection time windows (4 ns in our case; see Figure S6 in the Supporting Information).

Next, we applied p-MINFLUX to image a triangular arrangement of single-molecules separated by $d \approx 12$ nm in a DNA origami nanostructure, as depicted in Figure 3A. In this case, ATTO 532 was used because it shows appropriate blinking when inducing radical ion states in a reducing buffer for super-resolution blink microscopy (see the long blinking trace in Figure 3B).[25−27] Figure 3C shows the detected photons sorted according to their arrival times, relative to the laser sync signal, yielding four decays corresponding to the four excitation doughnuts. An expanded view of the fluorescence time trace in Figure 3B showing individual single-molecule emission events is depicted in Figure 3D. Each single-molecule event presents a different combination of intensity levels in the four detection channels, which encodes the fluorophore position. The integrated photon numbers in each detection

https://dx.doi.org/10.1021/acs.nanolett.0c04600
Nano Lett. XXXX, XXX, XXX−XXX

time window deliver the array of photon counts for each excitation doughnut $\overline{n}$ (as indicated by the colors in Figures 3C and 3D), which is then used to determine the molecular location.

Figure 3E shows the localization map obtained from the 100 s of measurement in Figure 3B. Single-molecule events with $N > 1200$ detected photons were considered. The threshold value of 1200 was chosen because it delivered a good compromise of localization precision (~2 nm) and frequency of events for this fluorophore and experimental conditions. The reconstructed image reveals three distinct populations in a triangular pattern that is in good agreement with the designed DNA origami structure. Suitable lower- and upper-intensity thresholds were used to discern single-molecule emission events from the background and multiple-molecule events, respectively (for details, see Supplementary Section 6 in the Supporting Information). The slice along the x-axis in Figure 3E is shown in Figure 3F, illustrating the achieved resolution. Two spots, separated by 11.3 nm, are clearly distinguishable (standard deviations of σ = 1.8 nm and σ = 2.1 nm). In addition, p-MINFLUX gives access to the fluorescence lifetime of each single-molecule detected, enabling the reconstruction of super-resolved fluorescence lifetime images, as shown in Figure 3G. For all localizations, the detected fluorescence lifetimes show a narrow distribution around an average value τ_{fl} = 3.9 ± 0.3 ns (Figure 3H).

Next, we tested the performance of p-MINFLUX for single-molecule tracking and multiplexing using fluorescence lifetime information. For this purpose, we used a dynamic DNA origami structure where three single-stranded DNAs protrude from the DNA origami platform with a separation distance of 6 nm between each strand, as indicated in the schemes of Figure 4A. The central protruding strand (also called pointer strand) can transiently hybridize to the other protruding strands (details in Supplementary Tables 3 and 4 in the Supporting Information). The end of the pointer strand is labeled with a single fluorophore, so that its position can be tracked via p-MINFLUX. Two DNA origami structures of this type were designed and fabricated. One was labeled with an ATTO 542 dye and had eight complementary nucleotides for transient binding (red, Figure 4A). The other was labeled with a Cy3B dye and had only seven complementary nucleotides for transient binding (blue, Figure 4A). As in any tracking experiment, temporal and spatial resolutions are linked and limited by the detected photon count rate. Being a single-photon counting technique, p-MINFLUX offers full flexibility to bin photons in time in order to optimize for time or spatial resolution, or a suitable compromise of both. In these experiments, we aimed to detect multiple transient bindings of the pointer strand, which imposes a requirement of minimum tracking time, different for each one of the two dynamic structures and limited by the fluorophore photostability. We ensured a localization precision of σ = 2−3 nm to clearly discern the two transient binding positions (x_0 = +6 nm, x_1 = −6 nm). This was achieved with a count rate of 20−60 kHz and time bins of 30−150 ms for ATTO 542, while for Cy3B we used a count rate of 20−110 kHz and time bins of 10−90 ms.

Figure 4B shows exemplary p-MINFLUX tracking traces for the two dynamic DNA origami structures. In both cases, the localizations of the fluorophores alternate between two positions separated by ~12 nm, as expected from the DNA origami design. Figure 4C shows the corresponding two-dimensional localization histograms. For the pointer labeled with ATTO 542, the two binding positions are found to be separated by 11.8 nm (σ = 2.2 nm), while for the pointer with Cy3B they are separated by 11.0 nm (σ = 2.5 nm).

By contrast, the transient binding times of the two structures differ significantly because of the different number of complementary nucleotides in the design. The pointer with eight complementary nucleotides (Figure 4B, top) presents binding times longer than the pointer with seven complementary nucleotides (Figure 4B bottom). Also, the two fluorophores used to label the pointers have distinct fluorescence lifetimes (Figure 4D).

Figure 4E shows a scatter plot of the average binding times versus fluorescence lifetimes of single DNA pointers labeled with ATTO 542 and Cy3B. The two structures are identifiable in this plot both by their distinct average binding times (T_B) of 1.92 and 0.37 s, and mean fluorescence lifetimes (τ_{fl}) of 3.2 and 2.6 ns, respectively. In Figure 4E, we also show simulations of the experiments (details in Supplementary Section 11 in the Supporting Information) in the background of the scatter plot. The simulations demonstrate that the experimentally observed variance in the binding times is dominated by the limited number of transitions detected for each structure before the fluorescent dye bleaches.

DISCUSSION AND CONCLUSIONS

We have presented p-MINFLUX, a new implementation of MINFLUX based on pulsed interleaved excitation and time-correlated single-photon counting. p-MINFLUX works under the same basic principle as the original MINFLUX and thus delivers equally photon-efficient single-molecule localizations, with its positive consequences for nanoscopy and tracking. We demonstrated localization precisions of $\sigma \approx 1-2$ nm with $N \approx 1000$ photons per localization, an improvement of ~10-fold compared to a typical camera-based localization. We demonstrated the performance of p-MINFLUX in the typical applications of molecular scale nanoscopy using blinking molecules as well as nanoscale tracking on DNA origami structures. In addition, p-MINFLUX is unique in providing access to excited-state lifetime information, enabling single-molecule identification (multiplexing) and FLIM nanoscopy with molecular-scale resolution; a 10−100 times improvement compared to previous works.[28,29] Fluorescence lifetime information may expand the field of application of p-MINFLUX, because it enables the specific detection of fluorescence in strongly scattering media.

In the first MINFLUX implementation, the subsequent excitations used to interrogate the position of single fluorophores were performed by shifting a laser focus with a scanner. To maximize scanning speed, an electro-optic scanner was used. By contrast, in p-MINFLUX, the excitation cycle is not limited by any optical scanner (~10−100 μs) but rather by the repetition rate of the pulsed laser, which corresponds to ~50 ns. Therefore, the time resolution is only limited by the detected emission rate, and ultimately by the decay lifetime of the emitter, holding potential for experiments exploring microsecond-scale dynamics. As an additional advantage, the setup can be regarded as a rather simple modification to a stage-scanning confocal microscope with pulsed excitation and TCSPC detection. Because of these advantages, we envision that p-MINFLUX will be more easily adopted and reproduced in other laboratories. To further facilitate this, all the instrumentation and data analysis Python code is available in

https://dx.doi.org/10.1021/acs.nanolett.0c04600
Nano Lett. XXXX, XXX, XXX−XXX

an open-source fashion. We note that a real-time adaptive arrangement of the excitation pattern, as demonstrated by Gwosch and co-workers,[16] can also be implemented in p-MINFLUX. This can be achieved, for example, by incorporating motorized mirror mounts. Also, photon efficiency can be maximized by the use of MINFLUX iterative approaches.[16]

In summary, p-MINFLUX constitutes a new analytical tool that combines molecular-scale spatial resolution with time-resolved lifetime measurements, which may be of use not only for ultraprecise single-molecule localization and nanoscopy, but also for new single-molecule energy transfer measurements such as FRET-, metal-, or graphene-induced energy transfer.

■ ASSOCIATED CONTENT

Supporting Information

The Supporting Information is available free of charge at https://pubs.acs.org/doi/10.1021/acs.nanolett.0c04600.

Details about the optical setups, the system for drift correction, the preparation of DNA origami samples, measurement of the excitation beam pattern and the point-spread functions, p-MINFLUX measurement protocol, position estimator and Cramér-Rao bound, p-MINFLUX simulations, effect of misalignment of the excitation beam pattern, crosstalk between detection time windows, and simulations of time traces of the pointer origami. Also, it contains a list of oligonucleotides used for each DNA origami used (PDF)

■ AUTHOR INFORMATION

Corresponding Authors

Philip Tinnefeld − *Department of Chemistry and Center for NanoScience, Ludwig-Maximilians-Universität München, 81377 München, Germany*; Email: philip.tinnefeld@cup.uni-muenchen.de

Fernando D. Stefani − *Centro de Investigaciones en Bionanociencias (CIBION), Consejo Nacional de Investigaciones Científicas y Técnicas (CONICET), C1425FQD Ciudad Autónoma de Buenos Aires, Argentina; Departamento de Física, Facultad de Ciencias Exactas y Naturales, Universidad de Buenos Aires, C1428EHA Ciudad Autónoma de Buenos Aires, Argentina*; orcid.org/0000-0002-3277-7215; Email: fernando.stefani@df.uba.ar

Authors

Luciano A. Masullo − *Centro de Investigaciones en Bionanociencias (CIBION), Consejo Nacional de Investigaciones Científicas y Técnicas (CONICET), C1425FQD Ciudad Autónoma de Buenos Aires, Argentina; Departamento de Física, Facultad de Ciencias Exactas y Naturales, Universidad de Buenos Aires, C1428EHA Ciudad Autónoma de Buenos Aires, Argentina*

Florian Steiner − *Department of Chemistry and Center for NanoScience, Ludwig-Maximilians-Universität München, 81377 München, Germany*

Jonas Zähringer − *Department of Chemistry and Center for NanoScience, Ludwig-Maximilians-Universität München, 81377 München, Germany*

Lucía F. Lopez − *Centro de Investigaciones en Bionanociencias (CIBION), Consejo Nacional de Investigaciones Científicas y Técnicas (CONICET), C1425FQD Ciudad Autónoma de Buenos Aires, Argentina*

Johann Bohlen − *Department of Chemistry and Center for NanoScience, Ludwig-Maximilians-Universität München, 81377 München, Germany*

Lars Richter − *Centro de Investigaciones en Bionanociencias (CIBION), Consejo Nacional de Investigaciones Científicas y Técnicas (CONICET), C1425FQD Ciudad Autónoma de Buenos Aires, Argentina; Department of Chemistry and Center for NanoScience, Ludwig-Maximilians-Universität München, 81377 München, Germany*

Fiona Cole − *Department of Chemistry and Center for NanoScience, Ludwig-Maximilians-Universität München, 81377 München, Germany*

Complete contact information is available at: https://pubs.acs.org/10.1021/acs.nanolett.0c04600

Author Contributions

[▽]These authors contributed equally to this work.

Author Contributions

The manuscript was prepared and written through the contributions of all authors. All authors have approved the final version of the manuscript.

Funding

This work has been supported by CONICET and ANPCYT Project Nos. PICT-2013-0792 and PICT-2014-0739. P.T. is grateful for support by the Deutsche Forschungsgemeinschaft (DFG, German Research Foundation) under Germany's Excellence Strategy − EXC 2089/1−390776260, and SFB1032. L.A.M. acknowledges a Ph.D. fellowship from CONICET and an exchange scholarship from the German Academic Exchange Service (DAAD). F.S. acknowledges support by the Boehringer Ingelheim Fonds. L.R. acknowledges funding from the German Academic Exchange Service (DAAD) and the German Academic Scholarship Foundation.

Notes

The authors declare no competing financial interest.

■ ACKNOWLEDGMENTS

F.D.S. acknowledges the support of the Max-Planck-Society and the Alexander von Humboldt Foundation.

■ REFERENCES

(1) Hell, S. W. Nanoscopy with Focused Light (Nobel Lecture). *Angew. Chem., Int. Ed.* **2015**, *54* (28), 8054−8066.

(2) Hell, S. W.; Sahl, S. J.; Bates, M.; Zhuang, X.; Heintzmann, R.; Booth, M. J.; Bewersdorf, J.; Shtengel, G.; Hess, H.; Tinnefeld, P.; et al. The 2015 Super-Resolution Microscopy Roadmap. *J. Phys. D: Appl. Phys.* **2015**, *48* (44), 443001.

(3) Sahl, S. J.; Hell, S. W.; Jakobs, S. Fluorescence Nanoscopy in Cell Biology. *Nat. Rev. Mol. Cell Biol.* **2017**, *18* (11), 685−701.

(4) Klar, T.; Hell, S. W. Subdiffraction Resolution in Far-Field Fluorescence Microscopy. *Opt. Lett.* **1999**, *24* (14), 954−956.

(5) Klar, T. A.; Jakobs, S.; Dyba, M.; Egner, A.; Hell, S. W. Fluorescence Microscopy with Diffraction Resolution Barrier Broken by Stimulated Emission. *Proc. Natl. Acad. Sci. U. S. A.* **2000**, *97* (15), 8206−8210.

(6) Rust, M. J.; Bates, M.; Zhuang, X. Sub-Diffraction-Limit Imaging by Stochastic Optical Reconstruction Microscopy (STORM). *Nat. Methods* **2006**, *3* (10), 793−796.

(7) Betzig, E.; Patterson, G. H.; Sougrat, R.; Lindwasser, O. W.; Olenych, S.; Bonifacino, J. S.; Davidson, M. W.; Lippincott-Schwartz, J.; Hess, H. F. Imaging Intracellular Fluorescent Proteins at Nanometer Resolution. *Science* **2006**, *313* (5793), 1642−1645.

(8) Hess, S. T.; Girirajan, T. P. K.; Mason, M. D. Ultra-High Resolution Imaging by Fluorescence Photoactivation Localization Microscopy. *Biophys. J.* **2006**, *91* (11), 4258−4272.
(9) Jungmann, R.; Steinhauer, C.; Scheible, M.; Kuzyk, A.; Tinnefeld, P.; Simmel, F. C. Single-Molecule Kinetics and Super-Resolution Microscopy by Fluorescence Imaging of Transient Binding on DNA Origami. *Nano Lett.* **2010**, *10* (11), 4756−4761.
(10) Schnitzbauer, J.; Strauss, M. T.; Schlichthaerle, T.; Schueder, F.; Jungmann, R. Super-Resolution Microscopy with DNA-PAINT. *Nat. Protoc.* **2017**, *12* (6), 1198−1228.
(11) Raab, M.; Schmied, J. J.; Jusuk, I.; Forthmann, C.; Tinnefeld, P. Fluorescence Microscopy with 6 Nm Resolution on DNA Origami. *ChemPhysChem* **2014**, *15* (12), 2431−2435.
(12) Strauss, S.; Nickels, P. C.; Strauss, M. T.; Jimenez Sabinina, V.; Ellenberg, J.; Carter, J. D.; Gupta, S.; Janjic, N.; Jungmann, R. Modified Aptamers Enable Quantitative Sub-10-Nm Cellular DNA-PAINT Imaging. *Nat. Methods* **2018**, *15* (9), 685−688.
(13) Xu, K.; Zhong, G.; Zhuang, X. Actin, Spectrin, and Associated Proteins Form a Periodic Cytoskeletal Structure in Axons. *Science* **2013**, *339* (6118), 452−456.
(14) Balzarotti, F.; Eilers, Y.; Gwosch, K. C.; GynnÅ, A. H.; Westphal, V.; Stefani, F. D.; Elf, J.; Hell, S. W. Nanometer Resolution Imaging and Tracking With Minimal Photon Fluxes. *Science* **2017**, *355* (6325), 606−612.
(15) Eilers, Y.; Ta, H.; Gwosch, K. C.; Balzarotti, F.; Hell, S. W. MINFLUX Monitors Rapid Molecular Jumps with Superior Spatiotemporal Resolution. *Proc. Natl. Acad. Sci. U. S. A.* **2018**, *115* (24), 6117−6122.
(16) Gwosch, K. C.; Pape, J. K.; Balzarotti, F.; Hoess, P.; Ellenberg, J.; Ries, J.; Hell, S. W. MINFLUX Nanoscopy Delivers 3D Multicolor Nanometer Resolution in Cells. *Nat. Methods* **2020**, *17* (2), 217−224.
(17) Pape, J. K.; Stephan, T.; Balzarotti, F.; Büchner, R.; Lange, F.; Riedel, D.; Jakobs, S.; Hell, S. W. Multicolor 3D MINFLUX Nanoscopy of Mitochondrial MICOS Proteins. *Proc. Natl. Acad. Sci. U. S. A.* **2020**, *117* (34), 20607−20614.
(18) Testa, I.; D'Este, E.; Urban, N. T.; Balzarotti, F.; Hell, S. W. Dual Channel RESOLFT Nanoscopy by Using Fluorescent State Kinetics. *Nano Lett.* **2015**, *15* (1), 103−106.
(19) Isbaner, S.; Karedla, N.; Kaminska, I.; Ruhlandt, D.; Raab, M.; Bohlen, J.; Chizhik, A.; Gregor, I.; Tinnefeld, P.; Enderlein, J.; et al. Axial Colocalization of Single Molecules with Nanometer Accuracy Using Metal-Induced Energy Transfer. *Nano Lett.* **2018**, *18* (4), 2616−2622.
(20) Kaminska, I.; Bohlen, J.; Rocchetti, S.; Selbach, F.; Acuna, G. P.; Tinnefeld, P. Distance Dependence of Single-Molecule Energy Transfer to Graphene Measured with DNA Origami Nanopositioners. *Nano Lett.* **2019**, *19* (7), 4257−4262.
(21) Müller, B. K.; Zaychikov, E.; Bräuchle, C.; Lamb, D. C. Pulsed Interleaved Excitation. *Biophys. J.* **2005**, *89* (5), 3508−3522.
(22) Thompson, R. E.; Larson, D. R.; Webb, W. W. Precise Nanometer Localization Analysis for Individual Fluorescent Probes. *Biophys. J.* **2002**, *82* (5), 2775−2783.
(23) Sigal, Y. M.; Zhou, R.; Zhuang, X. Visualizing and Discovering Cellular Structures with Super-Resolution Microscopy. *Science* **2018**, *361* (6405), 880−887.
(24) Dempsey, G. T. G. G. T.; Vaughan, J. C. J. J. C.; Chen, K. H. K.; Bates, M.; Zhuang, X. Evaluation of Fluorophores for Optimal Performance in Localization-Based Super-Resolution Imaging. *Nat. Methods* **2011**, *8* (12), 1027−1036.
(25) Vogelsang, J.; Kasper, R.; Steinhauer, C.; Person, B.; Heilemann, M.; Sauer, M.; Tinnefeld, P. A Reducing and Oxidizing System Minimizes Photobleaching and Blinking of Fluorescent Dyes. *Angew. Chem., Int. Ed.* **2008**, *47* (29), 5465−5469.
(26) Vogelsang, J.; Steinhauer, C.; Forthmann, C.; Stein, I. H.; Person-Skegro, B.; Cordes, T.; Tinnefeld, P. Make Them Blink: Probes for Super-Resolution Microscopy. *ChemPhysChem* **2010**, *11* (12), 2475−2490.
(27) van de Linde, S.; Krstić, I.; Prisner, T.; Doose, S.; Heilemann, M.; Sauer, M. Photoinduced Formation of Reversible Dye Radicals and Their Impact on Super-Resolution Imaging. *Photochem. Photobiol. Sci.* **2011**, *10* (4), 499−506.
(28) Thiele, J. C.; Helmerich, D. A.; Oleksiievets, N.; Tsukanov, R.; Butkevich, E.; Sauer, M.; Nevskyi, O.; Enderlein, J. Confocal Fluorescence-Lifetime Single-Molecule Localization Microscopy. *ACS Nano* **2020**, *14* (10), 14190−14200.
(29) Castello, M.; Tortarolo, G.; Buttafava, M.; Deguchi, T.; Villa, F.; Koho, S.; Pesce, L.; Oneto, M.; Pelicci, S.; Lanzanó, L.; et al. A Robust and Versatile Platform for Image Scanning Microscopy Enabling Super-Resolution FLIM. *Nat. Methods* **2019**, *16* (2), 175−178.

https://dx.doi.org/10.1021/acs.nanolett.0c04600
Nano Lett. XXXX, XXX, XXX−XXX